

Manganese dioxide as wide adaptive ultrafast photonic device for pulsed laser generation

Xin-He Dou(窦鑫河), Zhen Chen(陈震), Chen-Yan Zhang(张辰妍), Xiang Li(李响), Fei-Hong Qiao(乔飞鸿), Bo-Le Song(宋博乐), Shan Wang(王珊), Hao Teng(滕浩), and Zhi-Guo Lv(吕志国)

Citation: Chin. Phys. B, 2024, 33 (**11**): 114202. DOI: 10.1088/1674-1056/ad71b5
Journal homepage: http://cpb.iphy.ac.cn; http://iopscience.iop.org/cpb

What follows is a list of articles you may be interested in

High stability and low noise laser-diode end-pumped Nd: YAG ceramic passively *Q*-switched laser at 1123 nm based on a $Ti_3C_2T_x$-PVA saturable absorber

Jia-Le Yan(闫佳乐), Ben Li(李奔), Guo-Zhen Wang(王国珍), Shun-Yu Yang(杨顺宇), Bao-Le Lu(陆宝乐), and Yang Bai(白杨)
Chin. Phys. B, 2023, 32 (**11**): 114212. DOI: 10.1088/1674-1056/acf495

Single-frequency linearly polarized *Q*-switched fiber laser based on Nb_2GeTe_4 saturable absorber

Si-Yu Chen(陈思雨), Hai-Qin Deng(邓海芹), Wan-Ru Zhang(张万儒), Yong-Ping Dai(戴永平), Tao Wang(王涛), Qiang Yu(俞强), Can Li(李灿), Man Jiang(姜曼), Rong-Tao Su(粟荣涛), Jian Wu(吴坚), and Pu Zhou(周朴)
Chin. Phys. B, 2023, 32 (**7**): 074203. DOI: 10.1088/1674-1056/acad6d

Antimonene-based saturable absorber for a soliton mode-locked and *Q*-switched fiber laser in the 2 μm wavelength region

H Ahmad, B Nizamani, M Z Samion, N Yusoff, and M F Ismail
Chin. Phys. B, 2023, 32 (**6**): 064205. DOI: 10.1088/1674-1056/ac891f

Giant saturation absorption of tungsten trioxide film prepared based on the seedless layer hydrothermal method

Xiaoguang Ma(马晓光), Fangzhen Hu(胡芳珍), Xi Chen(陈希), Yimeng Wang(王艺盟), Xiaojian Hao(郝晓剑), Min Gu(顾敏), and Qiming Zhang(张启明)
Chin. Phys. B, 2023, 32 (**3**): 034212. DOI: 10.1088/1674-1056/acaf2a

Sequential generation of self-starting diverse operations in all-fiber laser based on thulium-doped fiber saturable absorber

Pei Zhang(张沛), Kaharudin Dimyati, Bilal Nizamani, Mustafa M. Najm, and S. W. Harun
Chin. Phys. B, 2022, 31 (**6**): 064204. DOI: 10.1088/1674-1056/ac3ba9

Manganese dioxide as wide adaptive ultrafast photonic device for pulsed laser generation

Xin-He Dou(窦鑫河)[1], Zhen Chen(陈震)[1], Chen-Yan Zhang(张辰妍)[1], Xiang Li(李响)[1], Fei-Hong Qiao(乔飞鸿)[1], Bo-Le Song(宋博乐)[1], Shan Wang(王珊)[1], Hao Teng(滕浩)[2,†], and Zhi-Guo Lv(吕志国)[1,‡]

[1] *School of Physical Science and Technology, Inner Mongolia University, Hohhot* 010021, *China*
[2] *Beijing National Laboratory for Condensed Matter Physics, Institute of Physics, Chinese Academy of Sciences, Beijing* 100190, *China*

(Received 19 July 2024; revised manuscript received 20 August 2024; accepted manuscript online 21 August 2024)

Research on novel ultrafast photonic devices with wide adaptability has become important scientific technical means to realize both scheme innovation and performance breakthrough in fiber laser generation. As types of transition metal oxide, manganese dioxide (MnO_2) materials exhibit remarkable properties including high photothermal stability, strong oxidation resistance, and excellent optical properties, making them promising candidate for utilization as modulation devices in nonlinear optics and ultrafast optics fields. We investigate the impact of MnO_2-based saturable absorber (SA) on the pulse characteristics. The experiment reveals that MnO_2-based SA supports effectively pulsed laser generation in wide pump power range and large dispersion parameter space with signal-to-noise ratio more than 85 dB. As far as we know, the pump power response range is outstanding among the most of the reported pulsed lasers, which is attributed to the large modulation depth of MnO_2 SA. We also investigate the impact of dispersion on the characteristics of laser output, which is not involved in other similar works. This research indicates that MnO_2 as a photonic device has vast potential in advanced ultrafast optics.

Keywords: MnO_2, saturable absorber, large modulation depth, *Q*-switching, mode-locking

PACS: 42.55.Wd, 42.60.–v, 42.60.Fc, 42.60.Gd **DOI:** 10.1088/1674-1056/ad71b5

1. Introduction

Over the past few decades, passive mode-locked fiber lasers have enabled a growing number of applications, such as high-speed optical communication, precision measurement, and machining.[1–7] Research on high-performance ultrashort pulse laser generation has always been one of the important research subjects. Saturable absorbers (SAs) are crucial components within the cavity of such lasers for ultrashort pulse generation. However, the majority of the available mode-locked devices possess limited adaptability, making complicated parameter settings possible when dealing with diverse laser systems.[8–11] On the other hand, constrained by nonlinear optics characteristics from SAs, both long-term reliability and signal-to-noise ratio (SNR) hinder frontier application performance of pulsed lasers.[12–15] Consequently, research on novel ultrafast photonic devices with wide adaptability has become key scientific issue. Therefore, it is of great significance to explore novel layered materials and to develop ultrafast photonic devices for promoting the performance breakthrough in pulsed laser generation.

To achieve this goal, one of the main directions is to seek materials with notable nonlinear properties and use them to prepare SAs.[16–18] In 2009, Bao *et al.* first used graphene to fabricate SA and applied it in the generation of ultrafast fiber laser.[19] Three years later, topological insulators (TI) were also used as ultrafast modulation devices.[20] Later, metal organic frameworks (MOFs),[21] perovskite,[22] MXene[23] and many other materials are gradually applied to SAs, and research on the manufacture of optoelectronic devices has also gained a great deal of attention. Since then, various transition metal compounds were sequentially explored and exploited as mode lockers. Typically, Wang *et al.* first proved that ultrashort pulse can be generated by using transition metal dichalcogenides (TMDCs),[24] which offered a novel perspective for the design of ultrafast lasers. These materials have shown outstanding absorption efficiency and robust light-matter interactions, but suffer from prolonged recovery time and limited carrier mobility. Thus, it is urgent to further explore novel materials with excellent performance and stable properties for fabricating advanced photonic devices. For a long time, less attention has been paid to the possibility of converting transition metal oxides (TMOs) into photonic devices. Oxygen and sulfur are both members of group VIA in the periodic table, and they are located in adjacent periods. The similar electronic configurations (O: $1s^2 2s^2 2p^4$; S: $1s^2 2s^2 2p^6 3s^2 3p^4$) result in the close physical properties of their compounds. Therefore, it is reasonable to speculate that the TMOs should also be materials with excellent properties for pulsed laser generation. Moreover, most of the oxides are stable in nature and can adapt to the requirements of fiber

†Corresponding author. E-mail: hteng@iphy.ac.cn
‡Corresponding author. E-mail: lvzhiguo@imu.edu.cn

© 2024 Chinese Physical Society and IOP Publishing Ltd

lasers under different conditions. However, despite its immense potential, research on its applications in ultrafast optical devices has only recently commenced. Until 2017, Mao *et al.* first used Fe_3O_4 as SA,[25] which convinced researchers that the application of TMOs to realize performance breakthrough in fiber laser generation is a feasible path. Therefore, we decide to follow the idea, and ultimately identify manganese dioxide (MnO_2) as a potential candidate for an ultrafast photonic device and realizing pulsed laser generation. MnO_2 has been widely used in batteries, catalysts and other fields.[26] MnO_2 exhibits desirable properties, such as broadband saturated absorption response, adjustable band gap and narrow band gap width, which makes it have incomparable advantages in making saturated absorption devices. In addition, MnO_2 exhibits excellent photothermal stability, enabling high-power laser irradiation without sacrificing inherent material properties, thus ensuring long-term stable operation of fiber lasers. Despite progress has been made in the study of MnO_2-based ultrafast photonic devices,[27] there remains an urgent need for further investigation, such as laser characteristics in wide pump power range, and dispersion dependence in pulsed laser generation. In prior research, scholars predominantly concentrate on the potential of MnO_2 as SA and its output performance parameters in the laser, yet they merely stop at exploring its feasibility without delving deeper into its mechanisms and broader applications. Till now, no literature attempt to further explore the response dependence of SA devices on different dispersion and power. In fact, such an understanding is of paramount importance for development of lasers with a wide adaptive range, capable of catering to diverse operational requirements. More systematic investigation on nonlinear saturable absorption properties and potential application in pulsed laser generation are yet to be conducted because in a practically applied ultrafast photonic device with wide adaptability would be more desirable.

In this work, we fabricate the MnO_2-based SA by laser deposition technology. Both material properties and optical performance are characterized. With such an SA, we observe the consistent and stable microsecond pulse generation within the input power range from 90 mW to 500 mW. As far as we know, the pump power response range is in the forefront among the reported Q-switched lasers. The broad pump range signifies that the Q-switched pulse generation is insensitive to voltage fluctuations, making the MnO_2-based device well-suited for harsh engineering applications. Additionally, even under different dispersion conditions, we can achieve the stable mode-locking operation, signifying that the modulation device corresponds to large parameter space range for mode-locking and widespread adaptability for laser cavity parameter settings. In addition, the output signal exhibits an SNR more than 85 dB, signifying the robust mode-locking operation, which highlights the reliability of MnO_2 as an excellent photonic device in pulsed laser generation. In a word, these experimental results confirm that MnO_2-based photonic devices have widespread adaptability for laser cavity parameter settings in pulsed laser generation and have application value for the improvement of laser stability.

2. Experimental process

Figure 1(a) presents the diagram of the MnO_2 atomic structure. It can be seen that its crystal structure is an octahedron,[28] with the Mn atoms in the middle and the O atoms distributed at the vertices. To analyze the crystal structure, we test the Raman spectrum (instrument model: Renishaw invia) of MnO_2 materials. Figure 1(b) shows that there are six distinct characteristic peaks appearing in the points of 285 cm^{-1}, 393 cm^{-1}, 527 cm^{-1}, 575 cm^{-1}, 641 cm^{-1}, and 722 cm^{-1}. According to the literature,[29] the characteristic peak at 641 cm^{-1} corresponds to the Mn–O bond, while the others originate from the lattice vibrations. Then, we use x-ray photoelectron spectroscopy (XPS; instrument model: ThermoFisher 250xi) to analyze the composition and state of the sample. In Fig. 1(c), the double peaks located at 654.2 eV and 642.05 eV correspond to the spin-orbit splitting of Mn $2p_{1/2}$ and Mn $2p_{3/2}$, respectively, which indicates that Mn is mainly concentrated in the +4 valence state, aligning with the literature.[30] Among them, Mn $2p_{3/2}$ can be further split into three peaks located at 640.75 eV, 642.05 eV, and 643.35 eV, which are attributed to Mn^{4+} (yellow), Mn^{3+} (green), and Mn^{2+} (blue), respectively.[30–32] Figure 1(d) shows the XPS spectrum of O 1s, with a peak at 532.35 eV. O 1s can also be further split into three peaks, which are generated by lattice oxygen (yellow), oxygen vacancies (green), and absorbed oxygen (blue). It can be seen that the relative intensity of lattice oxygen is higher, while the other two peaks are not obvious, indicating that the sample preparation process introduces fewer oxygen defects.[33] The data presented above show that MnO_2 used in our work has great material properties, which are the basis for subsequent experiments.

Then an appropriate amount of MnO_2 suspension is taken out and coated on the end face of the fiber ferrule with the laser deposition method. The fiber ferrule connector with deposited MnO_2 is connected with another fiber ferrule connector through a fiber adapter, thus forming a MnO_2-based SA. To test its nonlinear saturation absorption characteristics, a homemade ultrashort pulsed laser source is used, with a central wavelength of 1569.87 nm and a repetition rate of 92.59 MHz. The measured data are fitted with the following formula:

$$T(I) = 1 - \alpha_0 \cdot \exp\left(-\frac{I}{I_{\text{sat}}}\right) - \alpha_{\text{ns}}, \tag{1}$$

where $T(I)$ is the transmission, α_0 is the modulation depth, α_{ns} is the nonlinear loss, I is the incident peak intensity, and

I_{sat} is the saturation intensity. In Fig. 2, it can be seen that the modulation depth is 31.2% while the saturation intensity is 4.22 MW/cm^2. As far as we know, the modulation depth in this work is the largest among the data reported in literature. The large modulation depth is helpful for the establishment of a stable pulse and the generation of self-starting, which will enhance the pulse formation mechanism in a wide range of pump power and dispersion in subsequent experiments.

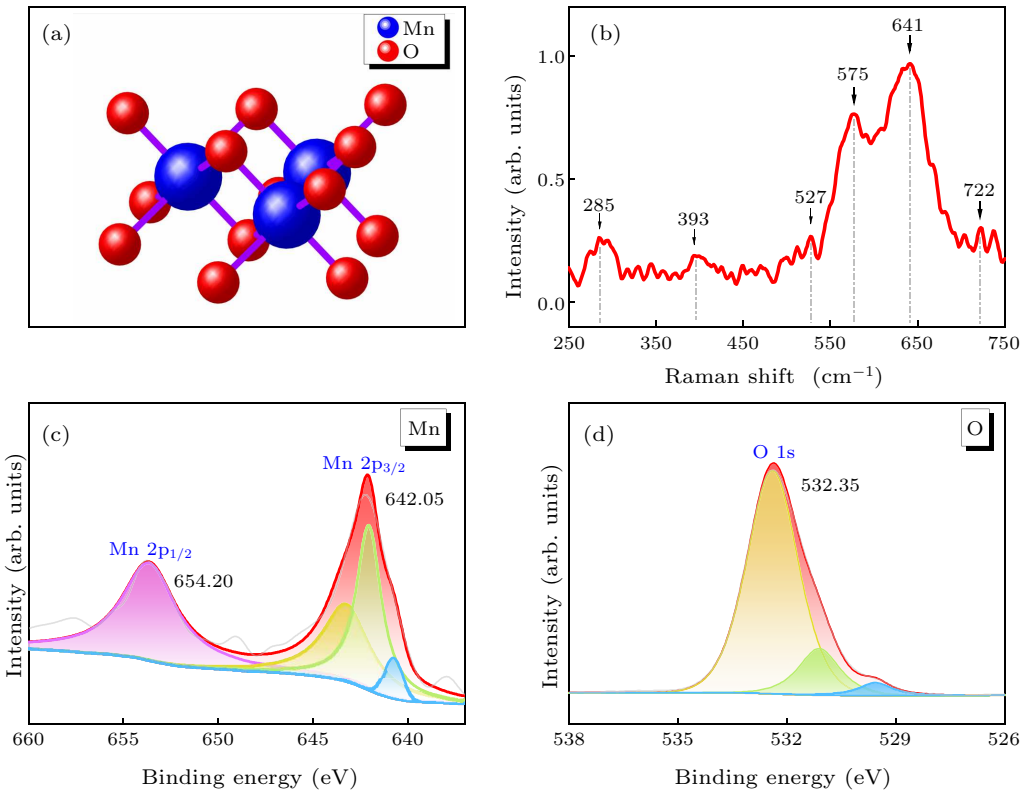


Fig. 1. Various material characterizations of the prepared MnO_2: (a) the ball-and-stick model of MnO_2; (b) Raman spectrum; (c) XPS spectrum for Mn 2p; (d) XPS spectrum for O 1s.

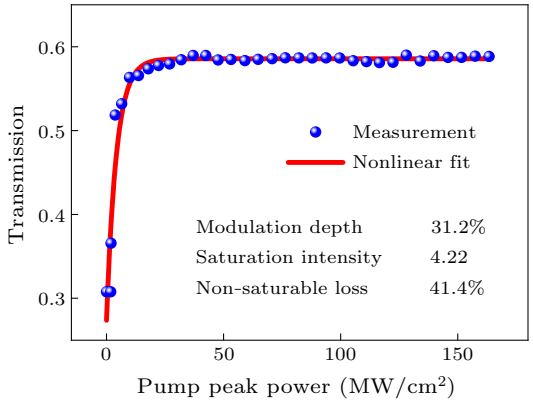


Fig. 2. Nonlinear optical transmission of the prepared MnO_2 SA.

The schematic diagram of the experimental setup is shown in Fig. 3. The 976 nm pump source (CONNET, VLSP-976-M-720-FA) outputs photonic signal, which passes through the pump protector and then is coupled into the ring cavity by a 980/1550 nm wavelength division multiplexer (WDM). The gain medium is an 80 cm-long erbium-doped fiber (EDF, 110-4/125). A polarization-independent isolator (PI-ISO) is set to guarantee unidirectional laser propagation in the ring cavity. The polarization controller (PC) is used to adjust the polarization state of the transmitted light. A 90 : 10 output coupler (OC) is employed to transmit photonic signals, enabling the detection of various parameters. In order to adjust the dispersion in the cavity, a single-mode fiber (SMF; smf-28e) is added into the cavity. The total length of the ring cavity is approximately 50.8 m, resulting in a net dispersion of -1.0904 ps^2. Oscilloscope (RIGOL, MSO8064), spectrum analyzer (YOKOGAWA, AQ6370D), radio-frequency (RF) spectrum analyzer (Kesight, N9010B), autocorrelator (A.P.E, SM2000), and power meter (OPHIR, 50(150) A-BB-26-V1) are utilized to assess the laser performance.

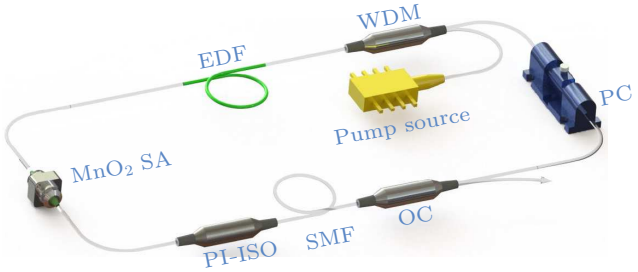


Fig. 3. Experimental setup for fiber laser based on MnO_2 SA. WDM: wavelength division multiplexor; MnO_2 SA: MnO_2-based SA; EDF: erbium-doped fiber; PI-ISO: polarization-independent isolator; PC: polarization controller; OC: output coupler; SMF: single-mode fiber.

3. Results

3.1. The *Q*-switched pulsed operation

When the pump power varies from 90 mW to 500 mW, stable *Q*-switched pulses can be observed with an oscilloscope. The centered wavelengths constantly locate at 1567.2 nm as the pump power increases. Figure 4(a) depicts the spectra at different power levels. From Fig. 4(b), it can be seen that the interval between adjacent pulses decreases from 109.4 μs to 23.76 μs with the increment in power. As the pump power increases, the time of accumulating sufficient cavity energy is reduced, thus generating a faster process of energy accumulation and release, which is manifested in the reduction of the period. Figure 4(c) exhibits a single pulse waveform at the pump power of 500 mW. The corresponding pulse width is 6.05 μs. Figure 4(d) depicts the RF spectrum. The fundamental repetition rate and the SNR are about 41.90 kHz and 69.5 dB, respectively.

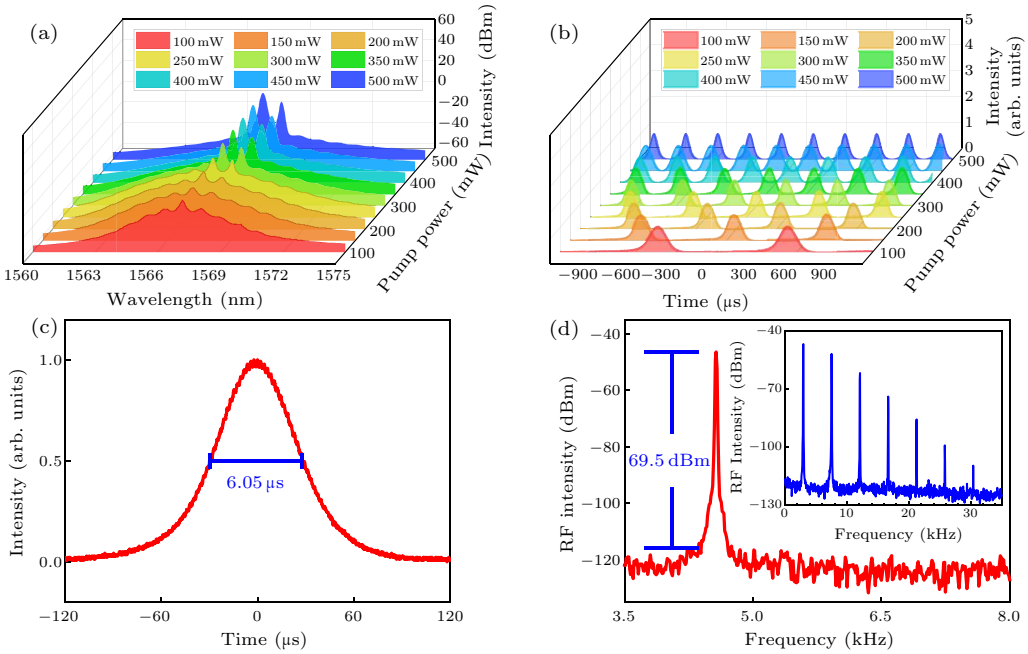


Fig. 4. Characteristics of passively *Q*-switched fiber laser: (a) spectra with different powers; (b) *Q*-switched sequences at different powers; (c) *Q*-switched pulse waveform; (d) RF spectrum.

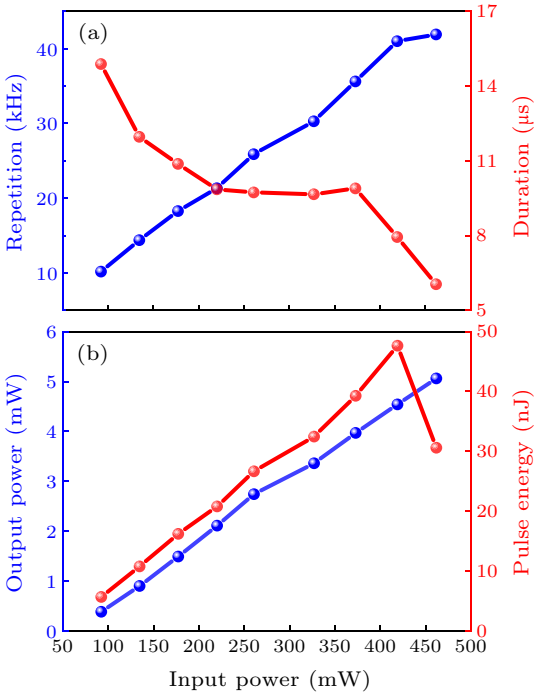


Fig. 5. (a) Variation curves of repetition rate (blue) and single pulse duration (red) corresponding to different input power; (b) output power (blue) and single pulse energy (red) under different input power.

In order to further study the influence of input power on the *Q*-switched properties, we conduct a thorough analysis in Fig. 5. Figure 5(a) shows that the repetition rate increases from 10.19 kHz to 41.9 kHz, while the duration of single pulse decreases from 14.9 μs to 6.05 μs. Evidently, there is a positive correlation between the input power and the repetition rate, while a negative correlation with the duration of the single pulse, which is consistent with the theoretical predictions.[34] In Fig. 5(b), it can be seen that almost linearly increased output power versus input power, and the corresponding slope efficiency is about 1.26% after fitting. The single pulse energy reaches a maximum value of 47.65 pJ at 419 mW input power (equivalent to 450 mW pump power).

3.2. The fundamental mode-locking operation

Then we adjust the length of the passive fiber to 40.1 m, and the corresponding net dispersion is calculated to be $-0.8726\ \text{ps}^2$. When the pump power reaches 500 mW, a stable periodic mode-locking operation can be observed by carefully adjusting the PC. Figure 6(a) depicts the oscilloscope trace of the pulse, and the pulse interval is about 204.6 ns. Figure 6(b) shows the RF spectrum. The fundamental frequency stands

at 4.887 MHz, with an SNR of more than 85 dB, indicating excellent stability of mode-locking operation. Figure 6(c) is the optical spectrum of the laser, with a central wavelength of 1559.81 nm and a 3 dB bandwidth of 1.22 nm. Notably, there are symmetric Kelly sidebands on both sides of the spectrum. The emergence of the phenomenon is attributed to the satisfaction of phase matching requirements, resulting in significant interference between solitons and dispersive waves (DWs) emitted by perturbed solitons when the phase difference is $2n\pi$. Figure 6(d) presents the autocorrelation trace and its corresponding sech^2 fitting curve. The measured pulse duration is 2.008 ps. The calculated time–bandwidth product (TBP) closely approaches the theoretical limit, indicating that the intracavity dispersion is almost completely compensated.

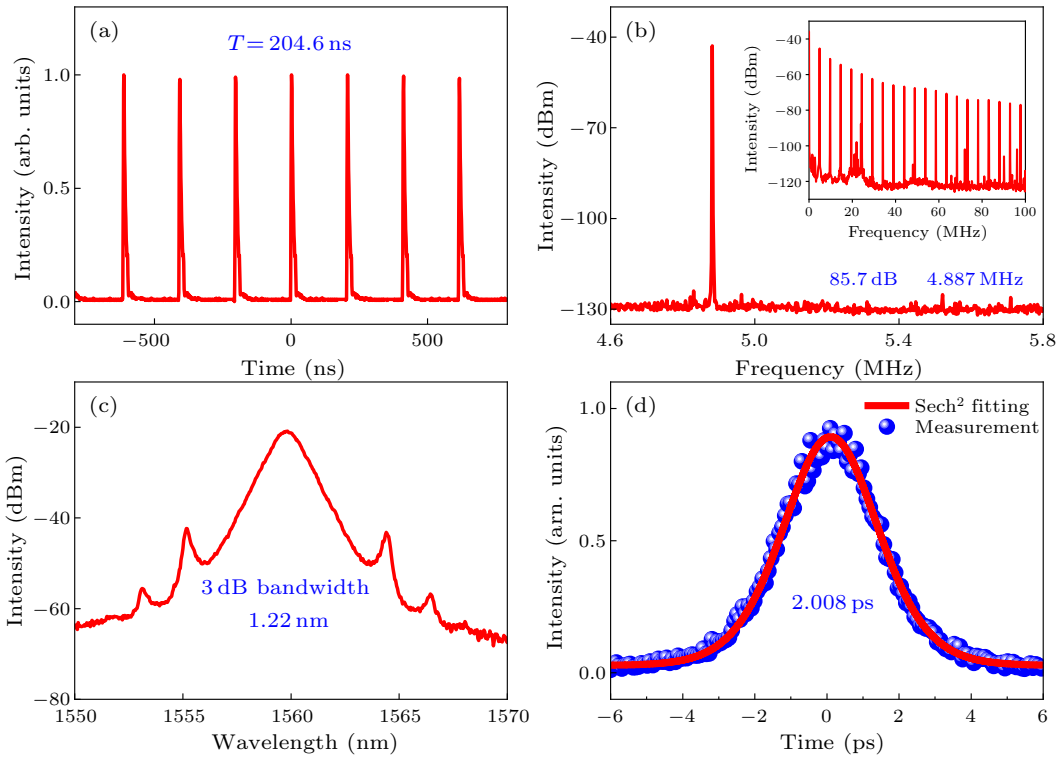


Fig. 6. Characteristics of passively mode-locked fiber lasers: (a) mode-locked pulse sequences; (b) RF spectrum near the fundamental frequency and RF spectrum within 100 MHz span; (c) spectrum of the laser; (d) autocorrelation trace and the corresponding sech^2 fitting curve.

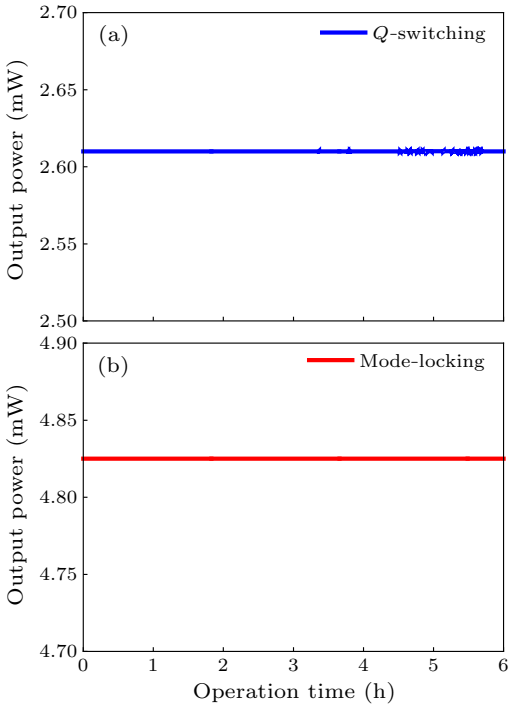


Fig. 7. Six-hour stability test of Q-switched and mode-locked outputs.

Subsequently, we continue to adjust the length of the passive fiber and achieve mode-locking operation with different dispersion: (1) By modifying the length of the passive fiber to 31 m, the net dispersion becomes -0.6724 ps^2. In this configuration, we achieve the mode-locking operation at 6.273 MHz fundamental repetition rates with an SNR of about 77 dB. The central wavelength and 3 dB bandwidth are 1560.17 nm and 1.09 nm, respectively. The corresponding pulse duration is 1.981 ps. (2) By adjusting the length of the passive fiber to 19 m, we obtain a net dispersion of -0.4084 ps^2. We achieve mode-locking operation at the fundamental frequency of 10.09 MHz with an SNR of 74 dB. The spectrum centers at 1560.06 nm with a 3 dB bandwidth of 1.56 nm. The pulse duration is 1.776 ps. It can be observed that as the length of passive fiber decreases, the dispersion gradually approaches 0, leading to the reduction of pulse duration.

Then, we summarize the data from the above experiments. As shown in Table 1, the numbers (Ⅰ, Ⅱ, Ⅲ) respectively represent experimental results in the paper, ordered from front to back. The listed data are three representative groups of data, and actually the mode-locking operation can be generated in a

wider dispersion adjustable range. The large parameter adjustment range represents a high tolerance for the balance between dispersion and nonlinearity, which makes the setting of laser components have more freedom. By varying the net dispersion within the cavity, we confirm that the MnO_2-based fiber lasers can operate in a large parameter space range. It is worth noting that the aforementioned experiments are all tested for stability over six hours. Figure 7 presents a six-hour stability test for *Q*-switching and the first group of mode-locking. It can be observed that the output power remains almost unchanged within this timeframe. To confirm whether the observed experimental phenomena are purely induced by MnO_2 SA, we replace the prepared SA with a clean fiber ferrule. In this case, no notable phenomenon is observed, indicating that the MnO_2 SA plays a pivotal role in pulsed laser generation.

Table 1. Three parameter adjustments and experimental data of passive mode-locked fiber lasers.

Parameters to be adjusted			
No.	Passive fiber length (including pigtail fiber) (m)	Ring cavity length (m)	Net cavity dispersion (ps^2)
Ⅰ	40.1	40.9	−0.8726
Ⅱ	31	31.8	−0.6724
Ⅲ	19	19.8	−0.4084

Experimental data						
No.	Period (ns)	Fundamental frequency (MHz)	SNR (dB)	Spectral center wavelength (nm)	3 dB bandwidth (nm)	Pulse duration (ps)
Ⅰ	204.6	4.887	85.7	1559.81	1.22	2.008
Ⅱ	159.4	6.273	77	1560.17	1.09	1.981
Ⅲ	99.02	10.09	74	1560.06	1.56	1.776

Table 2. Laser parameters based on different SA materials.

Q-switching						
No.	Type of SA	Pump power (mW)	Fundamental frequency (kHz)	SNR (dB)	Pulse width (μs)	References
1	graphene	13.5–73.7	10.36–41.8	30	Min 3.89	[35]
2	BP	50–185	6.983–15.78	45	Min 13.2	[36]
3	MoS_2	261–322	72.74–86.39	51.6	5.18–3.53	[37]
4	PdS_2	50.6–81.7	17.2–26.0	50	12.6–4.5	[38]
5	WS_2	–	79–97	44	Min 1.3	[39]
6	Bi_2O_3	104.9–244.5	28.41–49.51	51.28	4.9–1.55	[40]
7	Co_3O_4	55–165	29.8–70.92	60	10.9–5.02	[41]
8	NiO	25–95	19.57–52.18	55	Min 5.2	[42]
9	SnO_2	28–76	18.87–36.15	46.3	Min 10.7	[43]
		128–405	9.2–26.6	74	Min 4.08	
11	TiO_2	106–146	0.984–0.990	54	Min 9.74	[44]
12	ZnO	11.8–77.9	22.79–61.43	62	Min 7	[45]
13	MnO_2	90–500	10.19–41.9	69.5	14.9–6.05	this work
Mode-locking						
No.	Type of SA	Fundamental frequency (MHz)	SNR (dB)	Pulse width (ps)	3 dB bandwidth (nm)	References
1	graphene	10.9	40	3.2	0.8	[46]
2	CNT	10.61	75	22.73	0.3	[47]
3	Ag_2S	1.88	71.9	3.01	1.5	[48]
4	MoS_2	17.1	41	0.83	5.4	[48]
5	MoS_2	26.02	63	4.98	23.2	[49]
6	PtS_2	15.04	43	2.064	2.47	[50]
7	Sb_2S_3	3.47	54.3	2.4	2.1	[51]
8	RGO	7.47	70	18	–	[52]
9	V_2O_5	1	48.58	3.14	–	[53]
10	Fe_3O_4	2.806	57	2.93	1.39	[25]
11	MnO_2	16.24	55	0.9675	3.4	[27]
12		4.887	85.7	2.008	1.22	
13	MnO_2	6.273	77	1.981	1.09	this work
14		10.09	74	1.776	1.56	

4. Conclusion

Laser parameters based on different SA materials are summarized in Table 2. The presented result is outstanding in terms of the *Q*-switched pulse response range among the reported research literature, leading to wide adjustable range of fundamental frequency and pulse width. In addition, we

research the laser characteristics under different dispersion, which are not involved in previous works. As can be seen from Table 2, the MnO_2 SA exhibits superior pulse width and 3 dB bandwidth that are comparable to the most of the existing SAs. Moreover, its highlight also lies on the highest SNR among the listed materials when generating mode-locked pulses. As opposed to the current situation that most of the reported lasers can only operate within a very narrow range of dispersion, MnO_2-based SA exhibits unique adaptability and potential for the wide dispersion range. This experiment lays a solid foundation for subsequent research to delve deeper into the impacts of dispersion and power, and it provides novel insights for realizing the dynamic parameter configuration of lasers and the emergence of real-time adjustable lasers in the future. We believe that the transition metal oxides represented by MnO_2 have great prospects in large-scale practical applications of optical devices.

Acknowledgments

Project supported by the National Natural Science Foundation of China (Grant No. 12164030), Young Science and Technology Talents of Inner Mongolia (Grant No. NJYT22101), and the Central Government Guides Local Science and Technology Development Fund Projects (Grant No. 2023ZY0005).

References

[1] Li L, Xue Z, Pang L H, Xiao X S, Yang H R, Zhang J N, Zhang Y M, Zhao Q Y and Liu W J 2024 *Opt. Lett.* **49** 1293
[2] Li L, Cheng J W, Zhao Q Y, Zhang J N, Yang H R, Zhang Y M, Hui Z Q, Zhao F and Liu W J 2023 *Opt. Express* **31** 16872
[3] Cui W W, Xing X W, Chen Y Q, Xiao Y J, Ye H and Liu W J 2023 *Chin. Phys. Lett.* **10** 024201
[4] Xiao Y J, Xing X W, Cui W W, Chen Y Q, Zhou Q and Liu W J 2023 *Chin. Phys. Lett.* **40** 054201
[5] Wang H Y, Xiao Y J, Liu Q, Xing X W, Yang H J and Liu W J 2023 *Chin. Phys. Lett.* **40** 114204
[6] Meng X C, Li L, Sun N Z, Xue Z, Liu Q, Ye H and Liu W J 2023 *Chin. Phys. Lett.* **40** 124202
[7] Wang M X, Li P X, Xu Y T, Zhu Y C, Li S and Yao C F 2022 *Chin. Phys. Lett.* **39** 024201
[8] Shen J P, Huang X, Jiang S T, Jiang R R, Wang H Y, Lu P, Xu S C and Jiao M Y 2022 *Chin. Phys. Lett.* **39** 104201
[9] Lang Y, Peng Z Y and Zhao Z X 2022 *Chin. Phys. Lett.* **39** 114201
[10] Zhu G Y, Tian M F, Almokhtar M, Qin F F, Li B H, Zhou M Y, Gao F, Yang Y, Ji X, He S Q and Wang Y J 2022 *Chin. Phys. Lett.* **39** 123401
[11] Ma Y, Li W J, Xu Y F, Liu J Q, Zhuo N, Yang K, Zhang J C, Zhai S Q, Liu S M, Wang L J and Liu F Q 2023 *Chin. Phys. Lett.* **40** 014201
[12] Huang K W, Wang X, Qiu Q Y, Wu L and Xiong H 2023 *Chin. Phys. Lett.* **40** 104201
[13] Zhang X, Yi H H, Yao Y L, Wang S B and Shi L X 2023 *Chin. Phys. Lett.* **40** 124204
[14] Yi Q, Yang L L, Yang K, Li J, Du L, Huang B, Miao L L and Zhao C J 2021 *Opt. Express* **29** 41388
[15] Han Y, Gao B, Wen H, Ma C, Huo J, Li Y, Zhou L, Li Q, Wu G and Liu L 2024 *Light Sci. Appl.* **13** 101
[16] Han Y H, Li X H, Chen E C, An M Q, Song Z Y, Huang X Z, Liu X F, Wang Y S and Zhao W 2022 *Adv. Opt. Mater.* **10** 2201034
[17] Li L R, Li X H, Zhao Y, Feng J J, Zhang C X, Zhang Y, Shi Y, Ge Y Q and Zhang Y N 2022 *Nanotechnology* **33** 065203
[18] Han Y, Guo Y, Gao B, Ma C, Zhang R and Zhang H 2020 *Prog. Quantum Electron.* **71** 100264
[19] Bao Q L, Zhang H, Wang Y, Ni Z H, Yan Y L, Shen Z X, Loh K P and Tang D Y 2009 *Adv. Funct. Mater.* **19** 3077
[20] Zhao C, Zhang H, Qi X, Chen Y, Wang Z, Wen S and Tang D 2012 *Appl. Phys. Lett.* **101** 211106
[21] Sun Z H, Jiang X T, Wen Q, Li W J and Zhang H 2019 *J. Mater. Chem. C* **7** 4662
[22] Li P F, Chen Y, Yang T S, Wang Z Y, Lin H, Xu Y H and Li L 2017 *ACS Appl. Mater. Interfaces* **9** 12759
[23] Jiang X T, Li W J, Hai T, Yue R, Chen Z W, Lao C S, Ge Y Q, Xie G Q, Wen Q and Zhang H 2019 *npj 2D Mater. Appl.* **3** 34
[24] Wang S, Yu H, Zhang H, Wang A, Zhao M, Chen Y, Mei L and Wang J 2014 *Adv. Mater.* **26** 3538
[25] Mao D, Cui X Q, Zhang W D, Li M K, Feng T X, Du B B, Lu H and Zhao J L 2017 *Photon. Res.* **5** 52
[26] Pinky Y, Ayana B and Atul T 2023 *Chembioeng Rev.* **10** 510
[27] Li X H, Huang X Z, Han Y H, *et al.* 2023 *Ultrafast Sci.* **3** 0006
[28] Magnard N P L, Kirsch A, Jorgensen M R V, Kantor I, Sorensen D R and Huotari S 2023 *Inorg. Chem.* **62** 13021
[29] Wang Y H and Lv Y K 2016 *RSC Adv.* **6** 54032
[30] Cheng G, Yu L, Lin T, Yang R N, Sun M, Lan B, Yang L L and Deng F Z 2014 *J. Solid State Chem.* **217** 57
[31] Tang H, Chen W H, Li N, Hu Z L, Xiao L, Xie Y J, Xi L J, Ni L and Zhu Y R 2022 *Energy Storage Mater.* **48** 335
[32] Gu Y D, Min Y X, Li L, Lian Y B, Sun H, Wang D, Rummeli M H, Guo J, Zhong J, Xu L, Peng Y and Deng Z 2021 *Chem. Mater.* **33** 4135
[33] Yang R J, Guo Z J, Cai L X, *et al.* 2021 *Small* **17** 2170265
[34] Tao M M, Ye X S, Wang Z B, Wu Y, Wang P, Yang P L and Feng G B 2014 *Opt. Commun.* **319** 128
[35] Wang J Z, Luo Z Q, Zhou M, Ye C C, Fu H Y, Cai Z P, Cheng H Y, Xu H Y and Qi W 2012 *IEEE Photon. J.* **4** 1295
[36] Chen Y, Jiang G B, Chen S Q, Guo Z N, Yu X F, Zhao C J, Zhang H, Bao Q L, Wen S C, Tang D Y and Fan D Y 2015 *Opt. Express* **23** 12823
[37] Luo Z C, Wang F Z, Liu H, Liu M, Tang R, Luo A P and Xu W C 2016 *Opt. Eng.* **55** 081308
[38] Ping K, Cheng C, Tang T Y, Xin Y, Wang L H, Zeng Y and Hong T 2020 *Photon. Res.* **8** 511
[39] Zhang M, Hu G H, Hu G Q, Howe R C T, Chen L, Zheng Z and Hasan T 2015 *Sci. Rep.* **5** 17482
[40] Ahmad H, Aidit S N and Yusoff N 2018 *Infrared Phys. Technol.* **95** 19
[41] Nady A, Ahmed M H M, Numan A, Ramesh S, Latiff A A, Ooi C H R, Arof H and Harun S W 2017 *J. Mod. Opt.* **64** 1315
[42] Nady A, Ahmed M H M, Latiff A A, Numan A, Ooi C H R and Harun S W 2017 *Laser Phys.* **27** 065105
[43] Zhang L Y and Wang F 2023 *Opt. Fiber Technol.* **80**
[44] Reddy P H, Rahman M F A, Paul M C, *et al.* 2018 *Optik* **158** 1327
[45] Aziz N A, Latiff A A, Lokman M Q, Hanafi E and Harun S W 2017 *Chin. Phys. Lett.* **34** 044202
[46] Chang Y M, Kim H, Lee J H and Song Y W 2010 *Appl. Phys. Lett.* **97** 211102
[47] Zhou Y, Lin J, Zhang X Q, Xu L X, Gu C, Sun B, Wang A T and Zhan Q W 2016 *Photon. Res.* **4** 327
[48] Ahmed N, Omar S, Jusoh Z, Rahman H A, Dimyati K, Apsari R and Harun S W 2023 *Microw. Opt. Technol. Let.* **65** 365
[49] Khazaeizhad R, Kassani S H, Jeong H, Yeom D I and Oh K 2014 *Opt. Express* **22** 23732
[50] Long H, Tang C Y, Cheng P K, Wang X Y, Qarony W and Tsang Y H 2019 *J. Lightwave Technol.* **37** 1174
[51] Hu Q Y, Yang K J, Li M, Li P, Zhao H X, Zhang B, Liu J, Yang Y M and Chen X H 2023 *Nanotechnology* **34** 365203
[52] He X Y, Liu Z B, Wang D N, Yang M W, Liao C R and Zhao X 2012 *J. Lightwave Technol.* **30** 984
[53] Nady A, Baharom M F, Latiff A A and Harun S W 2018 *Chin. Phys. Lett.* **35** 044204